JOURNAL OF GEOPHYSICAL RESEARCH, VOL. 108, NO. D2, 4058, doi:10.1029/2002JD002575, 2003

Implementation of slope irradiance in Mesoscale Model version 5 and its effect on temperature and wind fields during the breakup of a temperature inversion

G. Hauge
Geophysical Institute, University of Bergen, Bergen, Norway

L. R. Hole
Norwegian Institute for Air Research, Kjeller, Norway

Received 27 May 2002; revised 25 September 2002; accepted 1 October 2002; published 24 January 2003.

[1] The atmospheric mesoscale model MM5 has been used at high horizontal resolution to simulate the breakup of a temperature inversion in complex topography. To improve the surface parameterizations during daytime, slope and orientation of the terrain have been taken into account in the calculation of short wave radiation at the surface. As the model resolution becomes higher, slope irradiance becomes increasingly important at high latitude. To evalute MM5 and slope irradiance's effect on the wind and temperature, a situation from 21 September 1994 is chosen. The situation is dominated by high pressure and no clouds, which gives the possibility of investigating the topography's effect on the radiation in greater detail. Compared to observations, results show improvement in both temperature and wind fields after the implementation of slope irradiances in MM5. The breakup period of the temperature inversion is also simulated more correctly. The RMS error is reduced by 35% for wind speed and 13% for temperature. This suggests that the influence of slope irradiance is larger for wind than for temperature in this situation. *INDEX TERMS:* 3307 Meteorology and Atmospheric Dynamics: Boundary layer processes; 3329 Meteorology and Atmospheric Dynamics: Mesoscale meteorology; 3359 Meteorology and Atmospheric Dynamics: Radiative processes; *KEYWORDS:* MM5, slope irradiance, temperature inversion

Citation: Hauge, G., and L. R. Hole, Implementation of slope irradiance in Mesoscale Model version 5 and its effect on temperature and wind fields during the breakup of a temperature inversion, *J. Geophys. Res.*, *108*(D2), 4058, doi:10.1029/2002JD002575, 2003.

1. Introduction

[2] It has been widely accepted that modeling of land surface processes plays an important role in mesoscale numerical models of the atmosphere [e.g., *Avissar and Pielke*, 1989; *Mahfouf et al.*, 1987]. Solar radiation is obviously an important factor in many aspects of surface forcing. To improve solar shortwave radiation parameterization, slope irradiance has been implemented into the nonhydrostatic mesoscale model MM5. The focus of this paper is slope irradiances and its effect on the wind and temperature fields during the breakup of a temperature inversion.

[3] General radiation processes on sloping surfaces has been thoroughly investigated by several authors [see, e.g., *Skartveit and Olseth*, 1986; *Oliver*, 1992; *Varley et al.*, 1996; *Kumar et al.*, 1997; *Duguay*, 1997]. These authors investigated radiative processes in general, but did not include this effect into numerical weather prediction models. Consideration of slope irradiance was introduced in a 3D atmospheric model by *Mahrer and Pielke* [1977]. Slope irradiance can, however, normally be neglected in numerical models when the horizontal model resolution is low (10 km or more) and the slopes are moderate. On the other hand, when the resolution is higher (less then 1–2 km), the effect of slopes might be considerable, especially at low solar zenith-angles and at high latitudes. Slope irradiance should, therefore, be included when the resolution becomes high and the terrain steep and undulating.

[4] The density of the observational network is normally unable to capture mesoscale and fine-scale meteorological structures. The majority of such structures are results of land surface forcings (topography, surface vegetation, soil moisture and other surface characteristics). Fine-scale nonhydrostatic numerical models, such as MM5, are tools to describe and forecast such structures. By using such models we get the possibility to obtain data outside observation points. An accurate and high resolution mesoscale model is therefore important if fine-scale meteorological structures are to be investigated. Increased computer capacity has made this possible during the last decade. Finer spatial and temporal resolutions and improved planetary boundary layer and surface parameterizations used in modern-era numerical mesoscale models permit more realistic simulations of both the diurnal and vertical structure of the PBL. Our focus has been on the description of the meteorological conditions rather than making forecasts.

0148-0227/03/2002JD002575$09.00

[5] During the last years there has been a rapid progress in model description of land surface processes and turbulence in the planetary boundary layer (PBL) [e.g., *Chen and Dudhia*, 2001a, 2001b; *Viterbo et al.*, 1999; *Oncley and Dudhia*, 1995]. Few physical parameterizations currently used in numerical models are thoroughly tested in the meso-γ area. During stable conditions with calm winds and fair weather, the quality of near surface predictions of wind and temperature depend less on the quality of boundary conditions and more on locally generated flow regimes. Such regimes, and the breakup of temperature inversions, are controlled by many factors [see, e.g., *Stull*, 1988; *Garrat*, 1999] such as turbulence, SW and longwave (LW) radiation, advection and subsidence.

[6] In the study presented here, model simulations with and without slope irradiance have been carried out in undulating terrain. The model results for wind and temperature have been compared to observed soundings carried out at Finnskogen NE of Oslo close to the Swedish border (see Figure 1).

[7] Five hundred meter grid distance in the finest nest gave sufficient terrain-gradients to see significant changes in the calculated patterns of shortwave radiation and temperature near the surface. Corresponding wind fields show large improvements in the lower part of the planetary boundary layer.

[8] Numerical model and setup for two simulations are presented in section 2. The implementation of slope irradiances in MM5 are described in section 3. In section 4 the results are given on the effects of the slope irradiance, both with and without slope irradiance implemented. Some conclusive remarks are given in section 5.

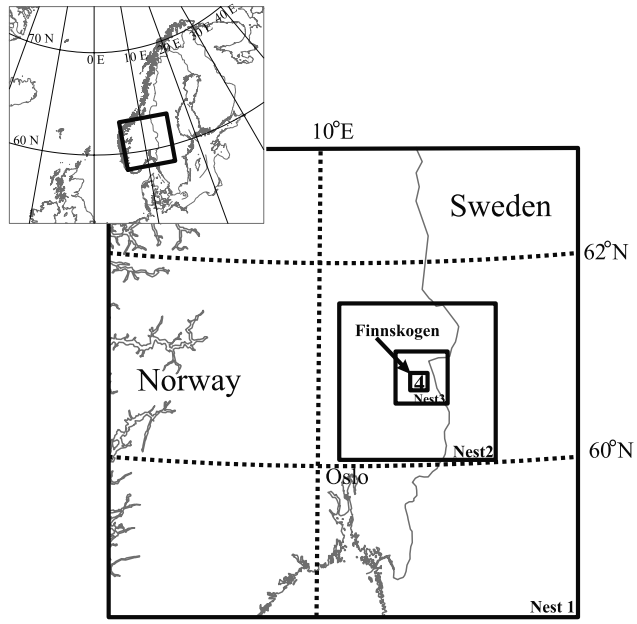

Figure 1. Nesting of MM5 domains. All domains are 40 × 40 grid points with the resolution 13.5 km ↔ 4.5 km ↔ 1.5 km ↔ 0.5 km (Nest1. . .Nest4). The upper left figure shows the position of Nest 1 on an European scale.

2. Model Setup

[9] The results presented are based on the fifth-generation mesoscale model, MM5V3.3 (hereafter MM5). MM5 is developed by PSU (Pennsylvania State University) and NCAR (National Center for Atmospheric Research) and is a mesoscale modeling system that includes advanced atmospheric physics. It is a mesoscale model (downloadable at http://www.mmm.ucar.edu/mm5/mm5-home.html) widely used for numerical weather prediction, air quality investigations and hydrological studies (*Warner et al.* [1991], *Grell et al.* [1994], *Mass and Kuo* [1998], *Chatfield et al.* [1999], *Chang et al.* [2000], etc.).

[10] MM5 is based upon a set of equations for a fully compressible non-hydrostatic atmosphere. Consequently it is possible to run it at fine horizontal and vertical scale corresponding to meso-γ scale (1–2 km). The model has the capability of multinesting and has here been nested in four steps from an ECMWF (European Centre for Medium Range Weather Forecast) analysis with approximately 40 kilometers between the grid points. The two-way interactive nesting has been done from 13.5 km ↔ 4.5 km ↔ 1.5 km ↔ 0.5 km (see Figure 1). This nesting procedure ensures that large-scale influence is captured in the model at the inner nest (Nest 4 with 0.5 km horizontal grid distance, see also Figure 1) and that finer scale structures influence the coarser nests. The number of grid-points were 40 × 40 for all domains and 31 vertical layers were used. The 31 vertical sigma levels are spaced so as to provide much higher vertical resolution in the planetary boundary layer than at upper levels (13 layers below 1000 meters).

[11] The initial and boundary conditions for the simulations are generated using the standard static initialization procedure for MM5, and first-guess fields are produced by interpolating data from ECMWF to the outer computational grid. The meteorological fields are further interpolated from the outer grid to the inner next domain until the finest nest at 500 meters horizontal grid distance.

[12] MM5 offers of a variety of different physical parameterization schemes for cumulus clouds, planetary boundary layer turbulence closure, radiation, explicit moisture, soil models and shallow convection. In the present simulations, the turbulence scheme based on *Hong and Pan* [1996] is used, coupled to an advanced land-surface model (LSM) described by *Chen and Dudhia* [2001a, 2001b]. For moisture an explicit moisture scheme, including the ice phase, was used [*Dudhia*, 1989]. The radiation scheme, based on *Dudhia* [1989], has been modified to take into account the effect of sloping surfaces (see section 3 for more details). For the outer domain (grid distance 13.5 km) a cumulus parameterization based on *Grell et al.* [1994] has been used. Topography and land-use were derived from the 1 km USGS (United States Geological Survey) data set [*Eidenshink and Faundeen*, 1998]. Further information on the model system is given by *Grell et al.* [1994].

[13] Simulations were made for 30 hours from an ECMWF analysis at 1200 UTC 20 September 1994, and updated by lateral boundary data every sixth hour. This allowed MM5 to get the proper daily variations in the PBL, even if the boundary data provided by ECMWF only gave small diurnal variation.

3. Implementation of Slope Irradiances

[14] Some aspects of the radiation scheme in MM5 are described in this section (for further details, see *Dudhia* [1989]), along with description of slope irradiance at the surface. The downward component of shortwave irradiance is estimated taking into account: (1) effects of solar zenith angle, which include the horizontal component of the irradiance; (2) clouds, with an albedo (cloud back scattering) and absorption; and (3) clear air, where there is scattering and water vapor absorption. In the model cloud fraction is either 0 or 1 in a grid box. Short Wave (SW) radiation [*Dudhia*, 1989] at the surface is originally calculated under the assumption of horizontal surfaces [*Dudhia*, 1989], i.e. SW radiation at the surface is a function of solar height [*Iqbal*, 1983] and a function, F, depending on transmissivity, water vapor, clouds and scattering, given as:

$$S = S_0 \sin h \cdot F. \tag{1}$$

S_0 is the solar constant, depending on the mean distance and the actual distance to the sun. The solar elevation is given as:

$$\sin h = \sin\delta \sin\phi - \cos\delta \cos\phi \cos\Omega, \tag{2}$$

where δ is Earth's declination, ϕ is geographic latitude in degrees (north positive) and Ω is the hour angle. This method of estimating the SW radiation may lead to considerable errors when the model resolution becomes high and the model terrain steep. Since our interest is sloping terrain, we have to split the global irradiance into its direct and diffuse components in order to describe the slope irradiance. This splitting is done according to a method developed by *Skartveit and Olseth* [1987], valid at high latitudes (>30°).

[15] When slope and orientation of the surface (the topography-azimuth angle), and the hourly diffuse and beam irradiances are known, the total irradiance on a surface inclined by an angle β towards an azimuth angle γ (orientation) can be written:

$$S(\beta,\gamma) = S_B \frac{\cos\theta}{\sin h} + \left(1 - \cos^2\frac{\beta}{2}\right)\alpha(S_D + S_B) + S_D(\beta,\gamma) \tag{3}$$

where h is solar elevation, β is ground slope (calculated using forward differences), and θ is the solar beam angle of incidence. $S_D(\beta, \gamma)$ is the diffuse sky irradiance, S_B is the direct radiation (beam) and $[1 - \cos^2(\beta/2)]\alpha$ $(S_D + S_B)$ is ground reflected irradiance. Negative $\cos\theta$ is replaced by zero in equation (3). This is a different approach than that of *Mahrer and Pielke* [1977], which did not require the splitting of SW radiation into direct and diffuse components. The splitting has the advantage of reducing the topographic effect in more cloudy conditions compared to *Mahrer and Pielke* [1977]. The solar beam angle of incidence can be written as [*Iqbal*, 1983]:

$$\cos\theta = \cos h \sin\beta \cos(\psi - \gamma) + \sin h \cos\beta, \tag{4}$$

which explains the correspondence between solar radiation and the orientation and slope of the underlying terrain. The solar azimuth is ψ where south is zero and east is positive. As in the original formulations [*Dudhia*, 1989], the effects of clouds and scattering are still taken into account in the calculations of S_D and S_B. It is clearly seen that for $\beta = 0$ (flat surface), $\cos\theta = \sin h$ (equation (4)). The solar radiation is then reduced to the original formulations [*Dudhia*, 1989]: $S = S_B + S_D$, i.e. S is the global irradiance on a horizontal grid box.

[16] To investigate the effect of SW radiation on meteorological conditions in the PBL, the surface energy budget has to be studied:

$$(1 - \alpha)S^{\downarrow} + L^{\downarrow} - L^{\uparrow} = H + L \cdot E_{tot} + G_0, \tag{5}$$

where α is the surface albedo, $S^{\downarrow}$ is incoming SW radiation described by equations (3) or (1), L is downward ($^{\downarrow}$) and upward ($^{\uparrow}$) long wave radiation, H is heat-flux, $L \cdot E_{tot}$ is latent heat-flux and G_0 is heat-flux down into the soil. H and $L \cdot E_{tot}$ is evaluated by using the difference between the surface and the lowest model layer (20 m). Surface temperatures are calculated according to the energy balance (equation (5)) and heating or cooling takes place whenever net incoming fluxes are positive or negative. The heat flux at the surface is thus naturally important in the energy budget and the corresponding surface temperatures.

[17] The modified radiation scheme increases the computational cost with 7 percent on a 16 processor model run (SGI Origin 3800 machine). This increase is seen when the radiation scheme is called every 10th minute (model time). The computation time is expected to increase or decrease depending on how often the radiation scheme is called.

4. Observations and Model Results

[18] In order to evaluate and compare model results with measured data, a situation from 21 September 1994 was chosen. As part of a large field campaign, extensive measurements with tethersonde were carried out during this day from 06 UTC to 16 UTC (07–17 local time) at Finnskogen in Hedmark County, NE of Oslo (Figure 1) (see *Hole et al.* [1998] for more details).

[19] The choice of situation was also based on the fact that little or no clouds were present this period. Effects of the changes in the radiation formulations can therefore be seen more directly.

[20] The ground near the observation site is undulating and the area is mostly covered with conifer forest, rising gradually from the river Glomma to the Swedish border. The observational point is assumed to be representative for domain 4 (500 meters grid distance), which is the area of interest in the model simulation. The area in and around the obsevation point is undulating and mostly covered with forest. Although the surface has moderate slopes in the observation point, the surface characteristics such as albedo and roughness are almost similar over domain 4. One can however not expect the meteorological conditions to be the same over the domain, since the topography are different.

[21] In the finest grid the lowest point is 220 meters and the highest 590 meters. With a 500 meter grid mesh (see Figure 2) the resulting slope ranges up to 20° with an overall average between 4–5°. The area around the observation site is relatively flat, with slopes in the order of 2–3° towards southwest.

[22] To test the effect of the changes made in the radiation scheme, two model runs are conducted. The first, called the

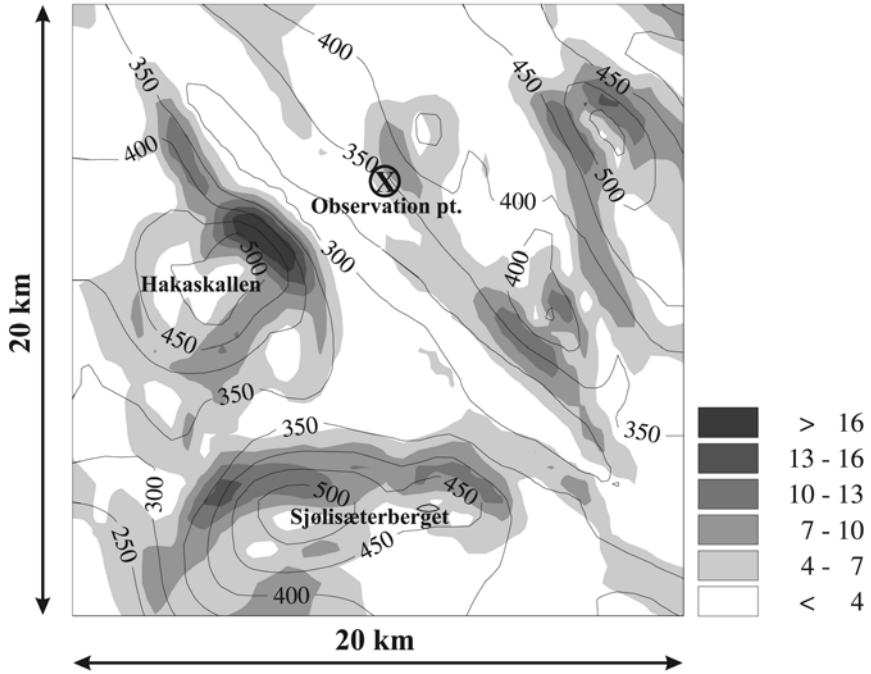

Figure 2. Shading: slope angles (degrees), lines: topography for Finnskogen, Nest 4. The x-mark indicates the observation site.

reference-run, used the original SW parameterizations based on *Dudhia* [1989], and the second, called the modified-run, had slope irradiance implemented.

[23] Analyses of mean Sea Level Pressure (MSLP) from the ECMWF boundary data are shown in Figures 3a and 3b, corresponding to the initial simulation time and 24 hours later. The situation was dominated by a high-pressure system situated over the main area at initial time (Figure 3a), which moved slowly toward southwest (Figure 3b). Only small pressure gradients were presented in the Finnskogen area during this period, leading to observations of low or moderate winds near the surface. We therefore assume that the meteorological conditions in the boundary layer at the inner domain mostly were forced by the physical processes described in equation (5), and less by synoptical scale.

4.1. Spatial Patterns of Shortwave Radiation

[24] The modeled SW radiation (W/m^2) are displayed on Figure 4. Equation (1) describes the parameterizations of SW in the original formulations. The only direct topo-

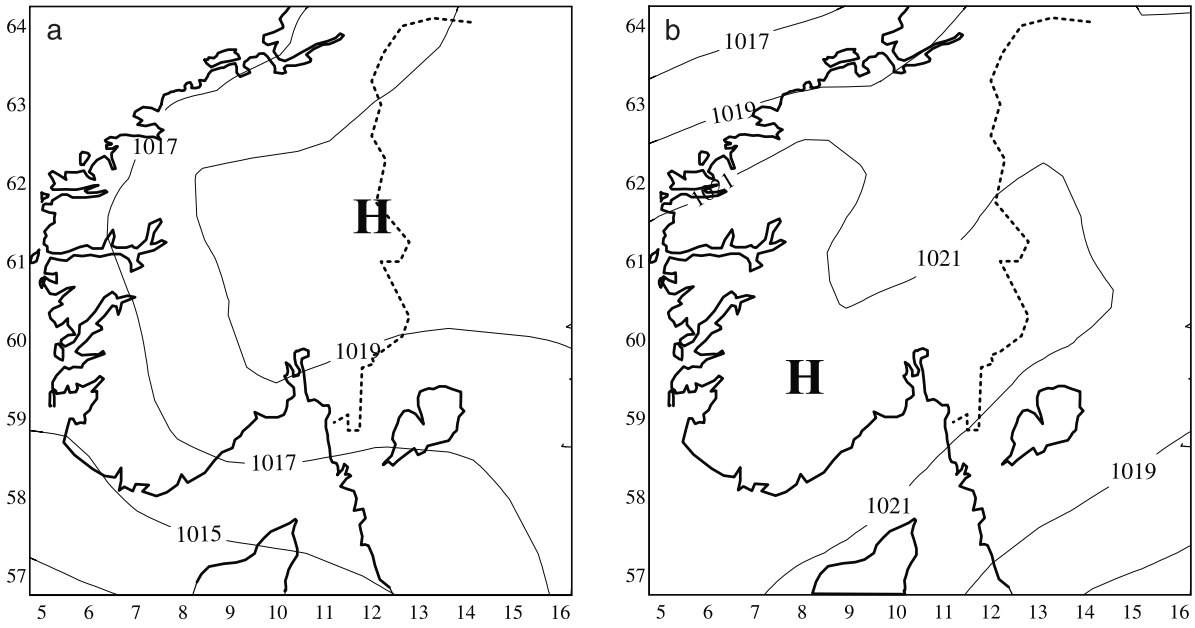

Figure 3. (a) Mean SLP at southern part of Norway 12 UTC 20 September 1994. (b) As Figure 3b, but at 12 UTC 21 Sept. Ticks at axes are latitude and longitude.

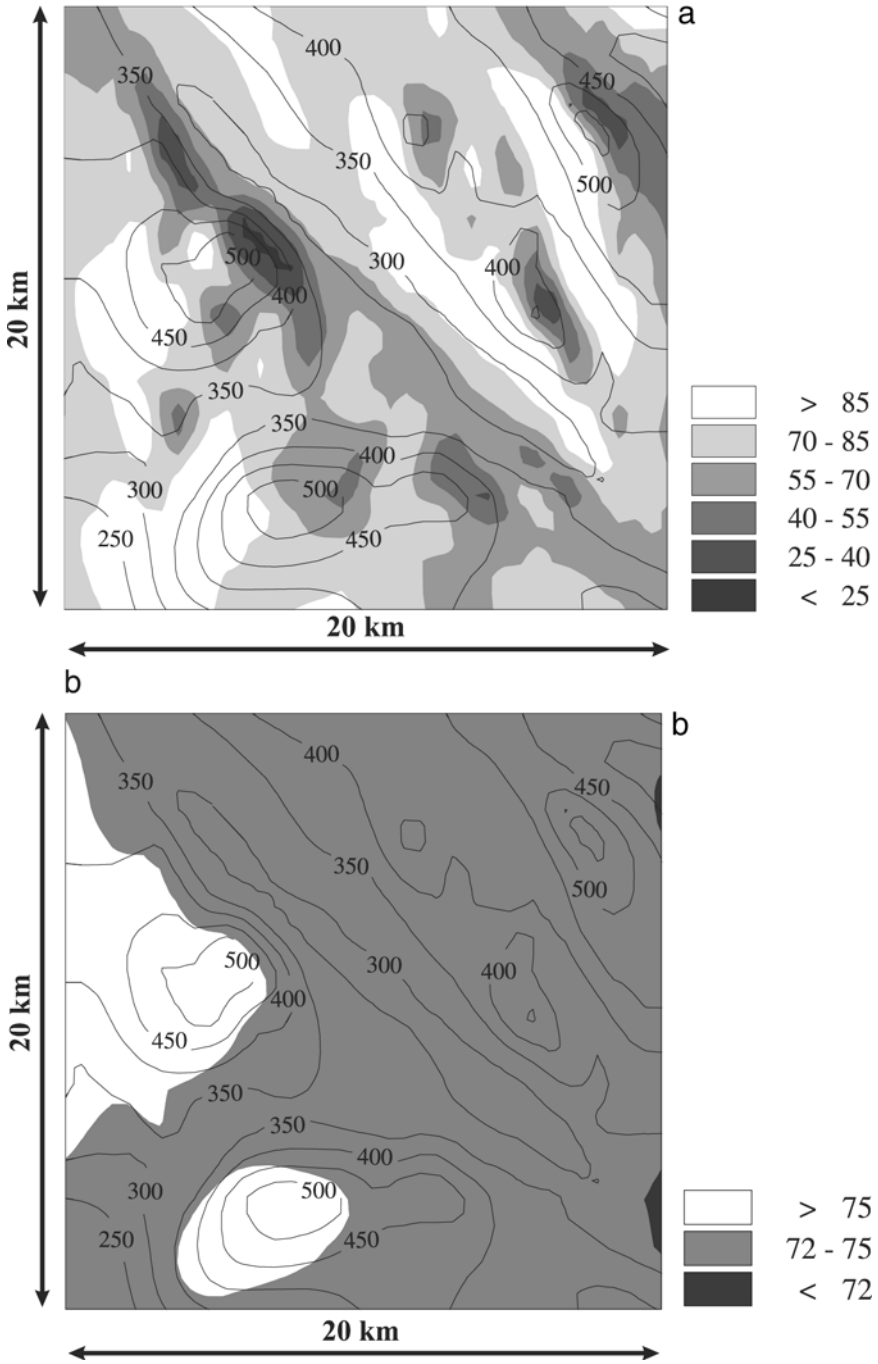

Figure 4. (a) Calculated net shortwave radiation (SW) at the surface, Wm^{-2}, in the modified-run at 16 UTC 20 September 1994. Shaded areas show minima of SW, white areas maximum. Isolines are height of topography. The model grid distance is 500 meters. (b) The reference run.

graphic effect that influences the solar height (sin h) in the reference run is therefore the terrain height. Since the atmosphere absorbs and scatters sun light, a point lying high in the terrain will get more radiation than a point lower in the terrain. This is demonstrated in Figure 4b. It is clearly seen (Figure 4a) that the direct radiation, S_B, is largest in areas oriented towards the sun, and the effect is naturally largest where the slopes are large (β is large, equation (3)). In areas oriented away from the sun cos $\theta = 0$, and the diffuse part (S_D) of radiation is the dominant part at the surface (last term of equation (3), right hand side).

[25] The large difference on the surface SW radiation demonstrates the influence of slope and orientation of topography on the SW calculations. The radiation minima's are reduced up to 70% compared to the reference run, and the maximums are up to 60% larger.

[26] The impact of model resolution on SW patterns has been investigated, by studying SW radiation on the second nest (Nest 2, see Figure 1). The grid distance is here 4.5 km, i.e. a large smoothing of model topography compared to the finest nest (500 m), and smaller slopes. Figure 5a shows the SW patterns in Nest 2 for the modified run at 4.5 km grid

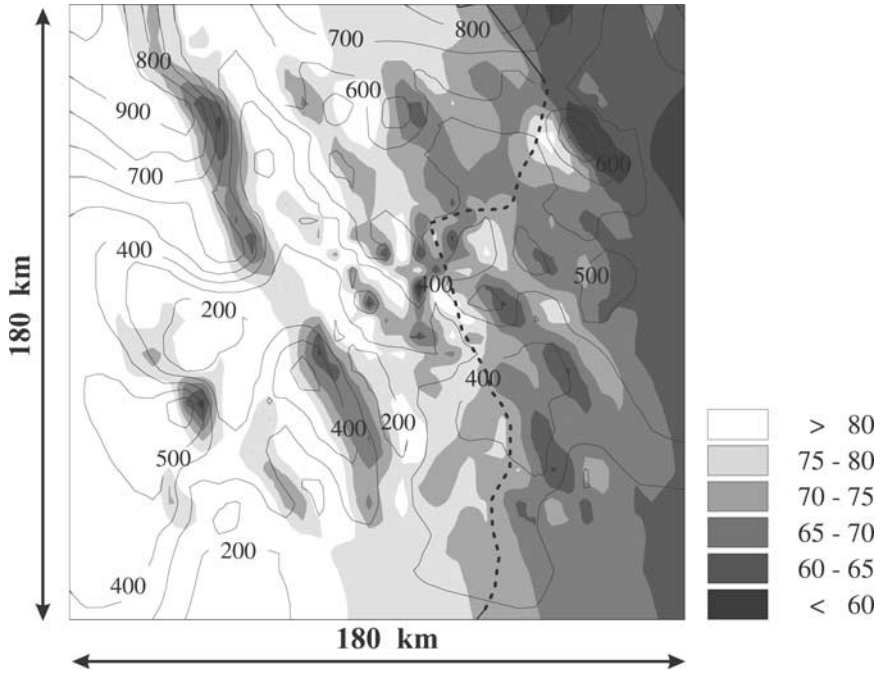

Figure 5. As Figure 4a, but for 4.5 kilometers grid distance (Nest 2 in Figure 1).

distance, revealing smaller differences than at 500 grid distance. An evident feature is the dependency of the solar height in the domain, giving more radiation in the western parts and in higher terrain. This variation is also seen in the reference run (not shown). Naturally the variation of the slopes and the SW radiation are very dependent of model resolution. This is clearly seen on Figures 4a and 5a, caused by sharper gradients in model terrain and larger variation of SW at high resolution. However, patterns of slope irradiances are still visible in the coarser domain.

[27] Similar distributions of SW can be seen at other times during the day, with larger differences between the reference and modified run in the morning and in the late afternoon.

4.2. Observed and Simulated (Reference) Temperatures

[28] The observed temperature soundings between 06 and 16 UTC (07–17 local time) are shown in Figure 6a, revealing a classical example of a morning temperature inversion breakup [see, e.g., *Stull*, 1988]. The figure clearly demonstrates how the ground was heated by solar radiation and how statically unstable air close to ground penetrates deeper into the inversion layer and destroys it from below. The observations do not indicate any influence of the free atmosphere (FA) above the PBL in the breakup. The FA influence on the inversion break up is described by many textbooks, e.g., *Stull* [1988] or *Garrat* [1999], in the explanation of the temperature inversion breakup, but is not seen in these observations. At 11 UTC, the atmospheric boundary layer stratification was close to neutral (constant potential temperature), indicating that the breakup of the inversion was completed.

[29] Simulated temperature soundings at the observation site for the reference run are shown in Figure 6b. The reference agrees well at 06 UTC and from noon. At 06 UTC both the shape of the inversion and the surface temperatures are as the observed. After 12 UTC the modeled neutral profiles are close to observed, although the temperatures are slightly too cold. The largest discrepancies are seen in the morning during the breakup of the inversion. At 06 and 07 UTC the errors are growing and the correspondence to observations is rather moderate, especially concerning the shape of the inversion. The inversion breakup is obviously faster in MM5 than in the observations. At 09 UTC observations still show an inversion from 130 m, while it has totally disappeared in the reference run.

[30] To evaluate the modeled inversion strength, a temperature gradient between 20 meters (lowest model level) and 100 m has been calculated (Figure 7, $\Delta T = T_{100m} - T_{20m}$). In the morning, the modeled breakup is more than one hour too early. The reason for this could be the absence of soil water melting, an effect not implemented in the land surface model of MM5 [*Chen and Dudhia*, 2001a, 2001b]. Melting of frozen water will slow down the heating process at the surface since energy is required to pass the "heat-capacity barrier."

[31] Another difference between the model results and the observations is the formation of a new inversion in the reference in the afternoon at 16 UTC. Clearly the new inversion is too strong and gives too steep gradients between 15 and 16 UTC (Figure 7) At sunset the surface is rapidly cooled, while there is a lag in this process in the real atmosphere. Evidently this process is not sufficiently resolved by MM5. One suggestion for this error is the parameterization of the soil heat flux (G_0 in equation (5)) in MM5, leading to a fast surface cooling. As SW radiation becomes low, there is a rapid response to the surface skin temperature. The temperature drop leads to a large heat flux into the soil since this flux depend on the difference between the soil temperature and the skin temp [*Chen and*

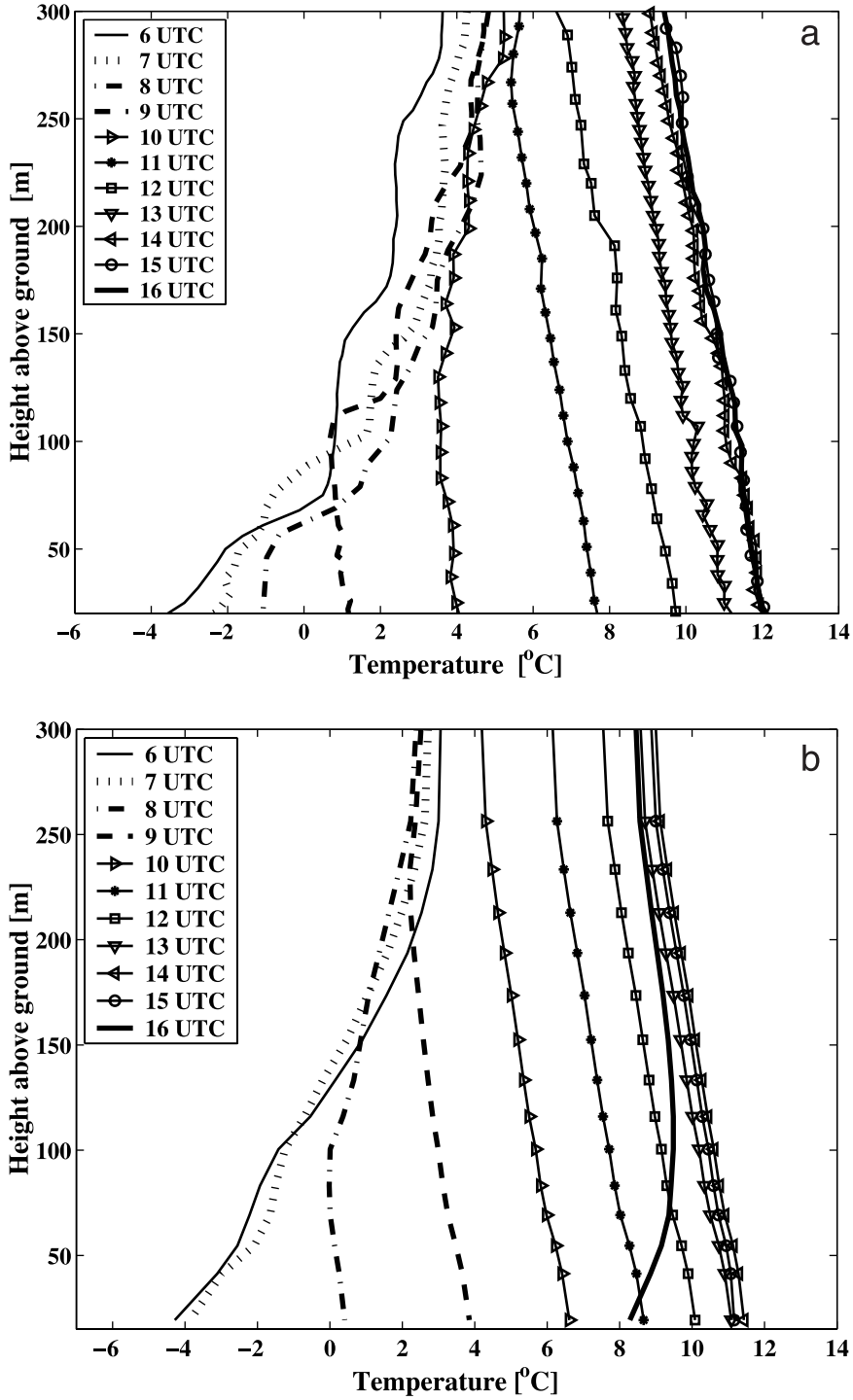

Figure 6. (a) Observed temperature soundings 21 September 1994 in the observation point marked at Figure 2. (b) Modeled sounding in the reference run.

Dudhia, 2001a, 2001b]. This results suggests that the energy-diffusion from the surface into the soil is too fast in MM5. Furthermore, the terrain slopes towards southwest, a fact that can be expected to have a slowing effect on the formation of a new inversion in the afternoon.

4.3. Temperatures in the Modified Run

[32] Only small changes can be seen in the modeled temperature soundings in the modified compared to the reference run (Figure 8). The reason is probably connected to small terrain slopes in the observation site (2–3 degrees). Still, two temperature profiles are evidently different from the reference run (Figure 8). The first is the change between 06 and 07 UTC when the modified run seems to give a more accurate breakup of the temperature inversion. The second is the reduced strength of the new inversion between 15 and 16 UTC. In the afternoon the observation area is oriented towards southwest giving less cooling than in the reference-

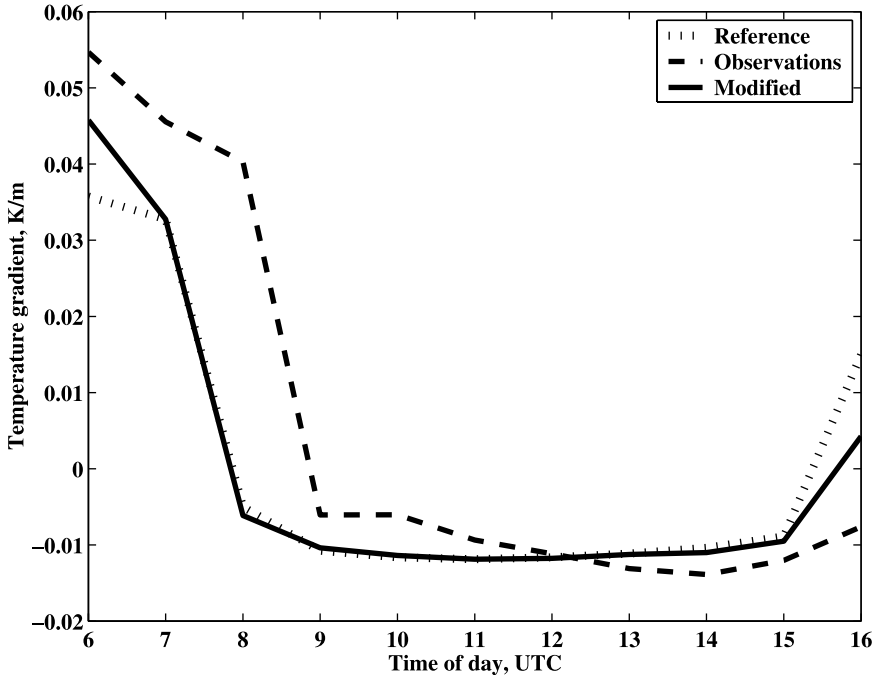

Figure 7. Time evolution of the temperature gradients between 100 and 20 meters, $T_{100m} - T_{20m}$. Positive values indicate the presence of an inversion.

run. In this way the tendency towards a new inversion is reduced.

[33] In the middle of the day there are only small differences between the two model runs. As in the reference run, the temperatures are slightly too warm in the middle of the day and too cold in the afternoon, compared to observations.

[34] The temperature gradients (Figure 7) are shown to be closer to the observed at 06 and 07 UTC in the modified run. The breakup of the inversion is still too fast in the modified run, and there are problems concerning the strength and shape of the inversion during the breakup period.

[35] In areas with large slopes the resulting temperature differences are influenced by slope irradiance. At 13 UTC 20 September (Figure 9a) the solar height is at its maximum, and the difference between the reference and the modified run is smaller. Evidently east-northeast of Hakaskallen, an area oriented away from the sun, it is cooler. On the west-southwest side it is warmer. NE of Hakaskallen

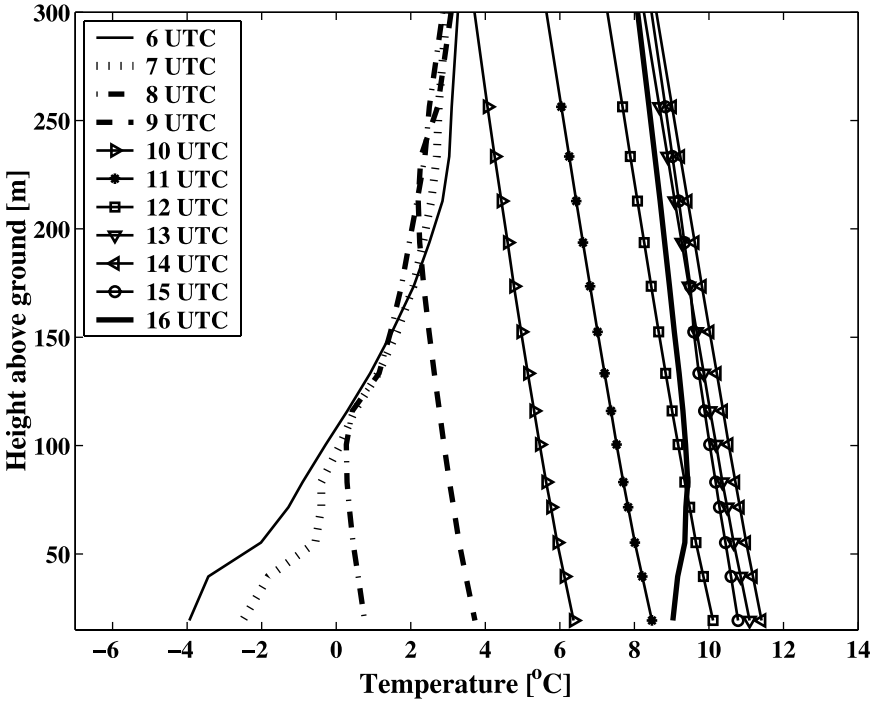

Figure 8. Modeled temperature soundings in the modified run.

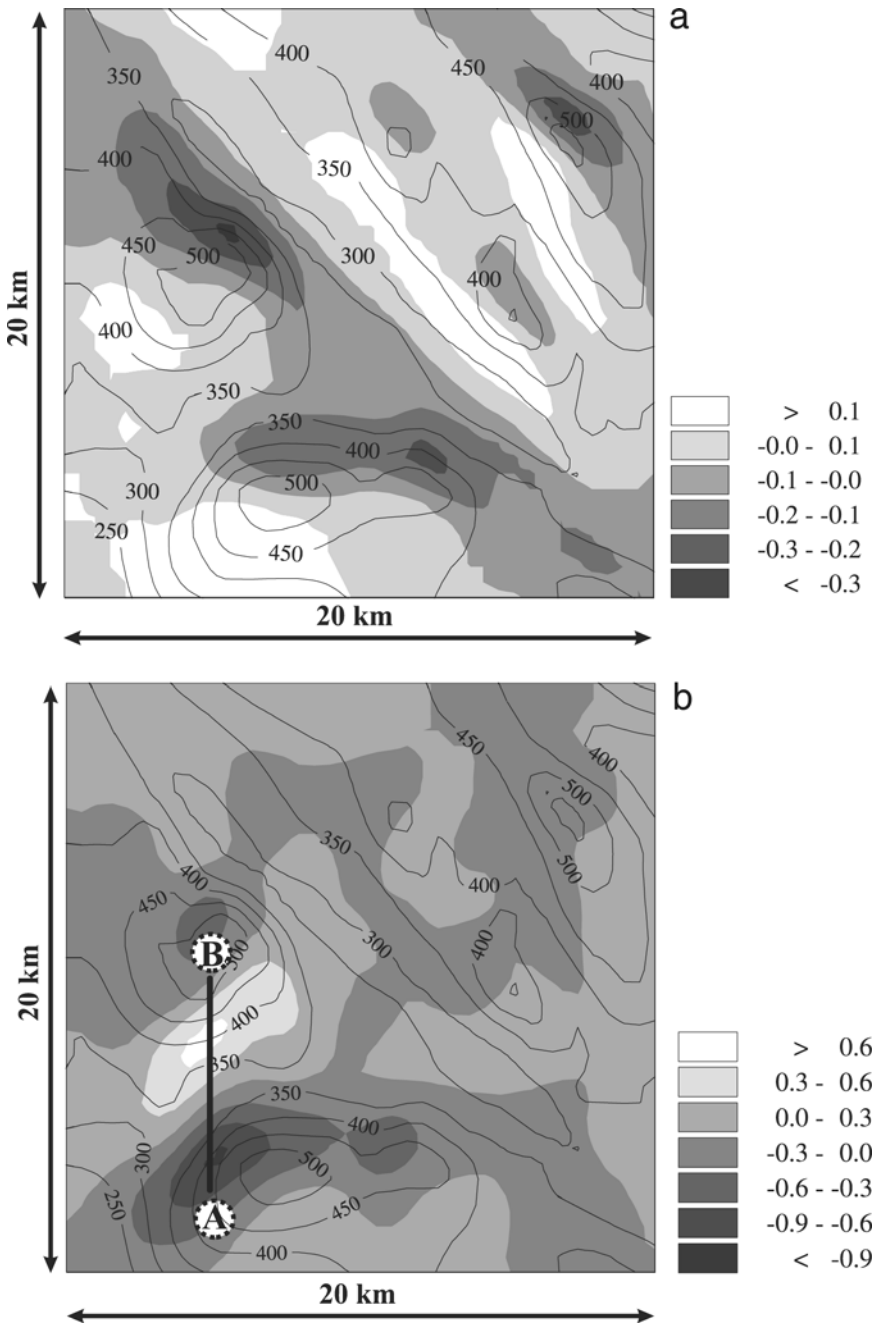

Figure 9. (a) Difference in temperature at the lowest model layer (20 meter) between the modified run and the reference run at 13 UTC 20 September 1994 ($T_{modified} - T_{reference}$). (b) As Figure 9a, but at 09 UTC 21.09. The marked line and with $A - B$ indicates the vertical cross-section shown on Figure 10.

cos θ (equation (4)) is negative (replaced by zero in equation (3)), and diffuse shortwave radiation is main contribution to the surface energy budget. I.e there is no direct SW radiation in this area. The warming on the west-southwest side is caused by a positive contribution from cos θ and the direct SW radiation. Similar patterns can be seen over the whole domain, enhancing the effect in steeper areas.

[36] The temperature differences at 09 UTC are shown in Figure 9b. The solar height is now lower, and relative temperature differences are larger than around noon. This cross-valley temperature difference ranges up to 1.5 degree. The largest difference between the modified and the reference run is seen on the shadow side of the valley, mainly caused by large terrain-gradients. A cross-section (indicated as a line on Figure 9b), showing the temperature difference between the modified and reference run, is illustrated on Figure 10. The temperature difference is about 1.5 K across the valley. The additional heating of the valley side gives rising motion in contrast the subsidence on the other side. This illustrates that the changed SW parameterization alters the local wind circulations.

4.4. Modeled and Observed Wind Speeds

[37] The observed wind speeds were less than 4 ms^{-1}, and the modeled wind speeds were even lower. Figure 11 shows the soundings for wind speeds from 11 to 14 UTC. It

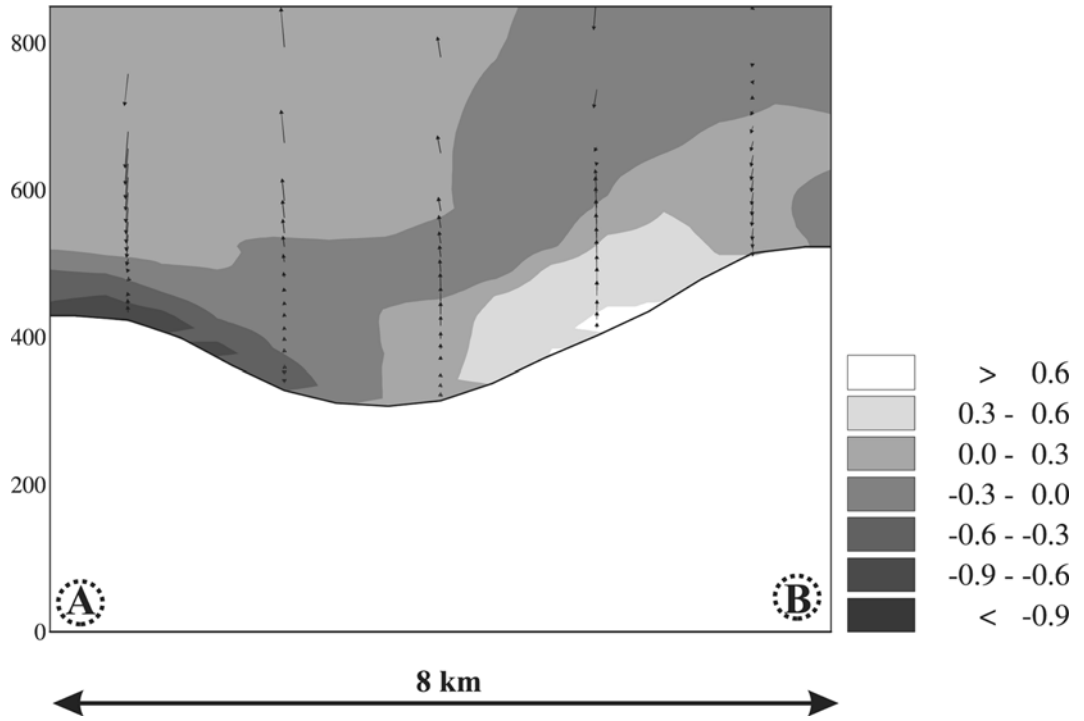

Figure 10. Vertical cross-section showing the temperature difference between the modified and the reference run at 09 UTC 21 September. The arrows indicate the vertical velocity in the cross-section, ranging from -1 to $+1$ ms^{-1} The cross-section is indicated on Figure 9b.

is clearly seen that the reference run gives a poor representation of reality. Largest errors are seen at 20 and 40 meters, since the modeled wind speeds approach to zero near ground. It is evident that the modified run gives a better estimate of the observed wind speeds. This is probably caused by the local circulation patterns set up in the surroundings (as in Figure 10).

4.5. Error Statistics

[38] Error statistics are a useful way to evaluate model results compared to observations. To evaluate the model results of wind speed and temperature, the root mean square errors (RMSE) have been computed [see, e.g., *Wilks*, 1995]. This sample of observational data is small, and the RMSE presented here is only meant as an indication of the improvements of the MM5 modifications.

[39] The RMS errors presented in Figure 12 are based on a the interpolated temperatures and wind speeds from 10 to 300 meters from 06 UTC to 16 UTC. The statistical analysis is done in discrete levels from 10 to 300 meters, and the RMSE at each level is calculated on the based on the observations from 06 UTC to 16 UTC, which gave 11 values at each vertical level.

[40] Figure 12a shows the RMSE in temperature, revealing an improvement throughout the entire lower boundary layer (up to 300 meters). The mean RMSE is reduced by 13% from the ground up to 300 meters for temperature and by 35% for the wind speed (Figure 12b). The increase of RMSE in temperature between 50 and 100 m is probably connected to the different shape of the modeled inversions compared to the observations. The modified run gives also here an improvement, and especially for the wind speed. The wind speed error is large near the surface where it becomes close to zero in both model runs.

5. Conclusions and Final Remarks

[41] The mesoscale model MM5 has been evaluated for its ability to reproduce and simulate the breakup of a temperature inversion. To improve the description of shortwave radiation at the surface (SW), slope irradiance has been implemented to take into account the slope and the orientation of the terrain.

[42] Results presented show improvements both in the modeled temperature and wind speeds when compared to observed soundings. After the modification, the daily temperature variation in the planetary boundary layer has better correspondence to observations, especially in the morning and in the afternoon. The RMSE in temperature was reduced by 13%. There are still some problems concerning the shape and strength in the breakup of the temperature inversion.

[43] The largest improvements are seen in the wind fields, where the RMSE are reduced with 35%. The large improvements are experienced because slope irradiance has greater influence in other areas of the domain. This forces local circulation patterns which also influences the observation point. This result might suggest that the influence of slope irradiance is greater on the wind fields than on the temperature fields, but the RMSE is not directly comparable. The temperature near the surface has close dependency on the local physical grid-point properties such as albedo and emissivity, while the effects on the wind fields can be more easily advected to other areas. Circulation set up in steeper

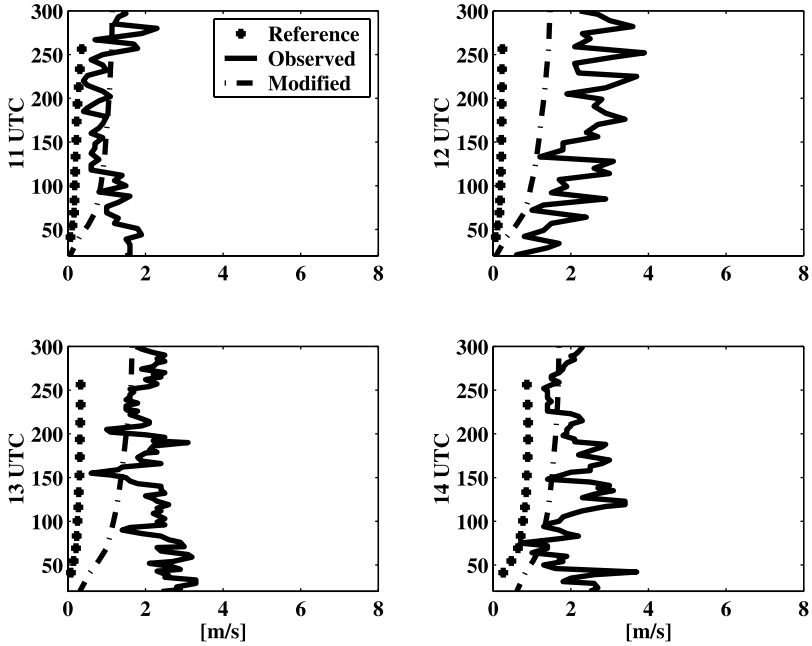

Figure 11. Observed and modeled profiles of wind speed (ms^{-1}) at the site marked on Figure 2.

areas can therefore have larger influence in other areas of the domain. Since the observation point indicates improved wind fields and the terrain is relatively flat in this area, it is reasonable to assume that the modified run represents an improvement over the whole domain.

[44] Surface fluxes are changed according to the new SW patterns. This causes the planetary boundary layer depth and the mixing heights to change in similar ways; areas with less SW radiation and smaller heat and moisture fluxes gets a reduction in the PBL height. The vertical velocities are influenced in a similar way, giving larger updraft or downdraft depending on net SW radiation. Even if improvements are seen in many ways in this simulation, slope irradiance could not be expected to have the same influence in more cloudy conditions. When more clouds are present the diffuse irradiance becomes the most dominant part of SW radiation and the topographic effect will be damped out.

[45] In spite of the improvements after the modifications, there are still unresolved problems concerning modeling of temperature inversions. During static stable conditions with calm winds and fair weather the quality of the near surface prognosis strongly depend on the parameterizations used in the planetary boundary layer and at the surface. The results presented here indicates that the breakup part of the inversion is a problem. Effects of the surface and its characteristics can have an impact on heat and moisture fluxes in the PBL. Soil water freezing is an important physical process to avoid errors around the melting point. Melting or freezing of water will slow down the heating or cooling process at the surface since energy is required to pass the "heat-

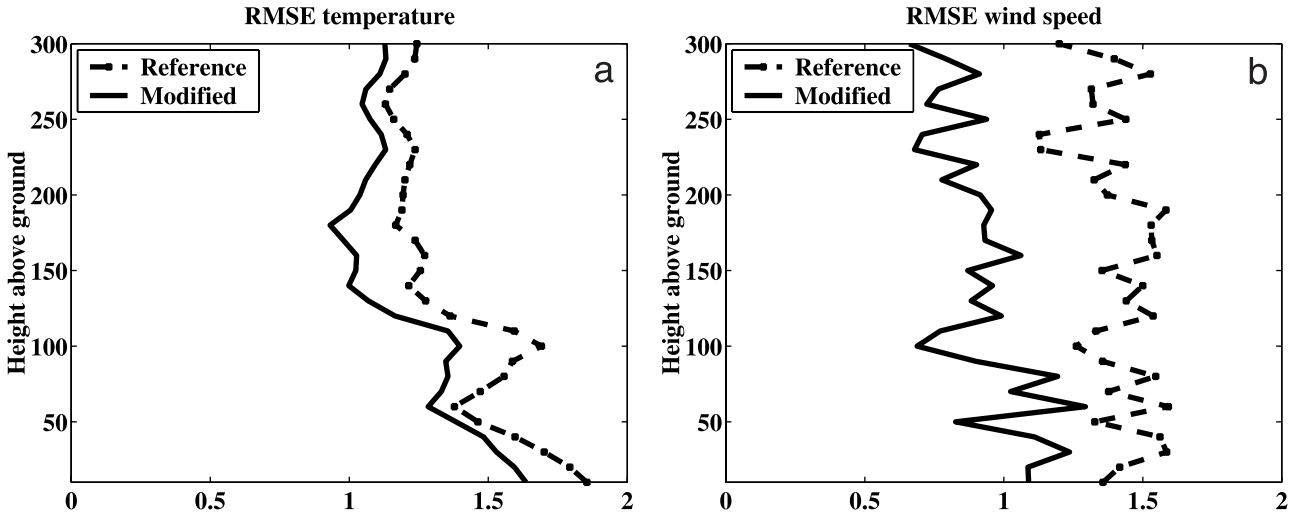

Figure 12. (a) RMSE in temperature between 06 UTC and 16 UTC 21 September. (b) RMSE in wind speed.

capacity barrier''. Freezing and melting of soil water should therefore be included into MM5 in the future. A more accurate description of the surface properties can therefore improve the flux estimation in the boundary layer. These fluxes are further coupled to the turbulence parameterizations used in the model. Other formulations of turbulence can lead to different solutions.

[46] More tests with other surface conditions, such as snow cover, should be performed before any firm conclusions on the usefulness of the modifications can be drawn. In addition, studies of how the modifications will influence the results in more cloudy conditions remain to be investigated.

[47] **Acknowledgments.** This study has been supported by the Norwegian Defence Construction Service, Environmental Section. The authors would like to thank S. Grønås for valuable suggestions for improvement of early versions of the manuscript and J. A. Olseth for interesting discussions and help to implement slope irradiance in MM5. We also thank K. J. Barret for help with the writing of this manuscript. The meteorological field campaign which provided the data was led by Y. Gjessing and engineer Tor de Lange, Geophysical Institute, University of Bergen. Supercomputing resources were made available by the Norwegian Research Council. Comments from reviewers are also greatly appreciated.

References

Avissar, R., and R. Pielke, A parameterization of heterogeneous land surfaces for atmospheric numerical models and its impact on regional meteorology, *Mon. Weather Rev.*, *107*, 2113–2136, 1989.

Chang, D., L. Jiang, and S. Islam, Issues of soil moisture coupling in MM5: Simulation of the diurnal cycle over the FIFE area, *J. Hydrometeorol.*, *1*(6), 477–490, 2000.

Chatfield, R., J. Vastano, L. Li, G. Sachse, and V. Connors, The Great African Plume from biomass burning: Generalizations from a three-dimensional study of TRACE A carbon monoxide, *J. Geophys. Res.*, *103*(D21), 28,059–28,077, 1999.

Chen, F., and J. Dudhia, Coupling an advanced land-surface/hydrology model with the Penn State/NCAR MM5 modeling system, part I, Model implementation and sensitivity, *Mon. Weather Rev.*, *129*, 569–585, 2001a.

Chen, F., and J. Dudhia, Coupling an advanced land-surface/hydrology model with the Penn State/NCAR MM5 modeling system, part II, Preliminary model validation, *Mon. Weather Rev.*, *129*, 587–604, 2001b.

Dudhia, J., Numerical study of convection observed during the winter monsoon experiment using a mesoscale two-dimensional model, *J. Atmos. Sci.*, *46*(20), 3077–3107, 1989.

Duguay, C., Radiation modeling in mountaionous terrain: Review and status, *Mt. Res. Dev.*, *13(4)*, 339–357, 1997.

Eidenshink, J., and J. Faundeen, The 1-km AVHRR global land dataset: First stages in implementation, *Int. J. Remote Sens.*, *15*, 3443–3462, 1998.

Garrat, J., *The Atmospheric Boundary Layer*, Cambridge Univ. Press, New York, 1999.

Grell, G., J. Dudhia, and D. Stauffer, A description of the Fifth-Generation Penn State/NCAR Mesoscale Model (MM5), *NCAR Tech. Note TN-398*, Natl. Cent. for Atmos. Res., Boulder, Colo., 1994.

Hole, L., Y. Gjessing, and T. Lange, Meteorological measurements and conditions during Norwegian trials, *Noise Control Eng. J.*, *46*(5), 199–207, 1998.

Hong, S., and H. Pan, Nonlocal boundary layer vertical diffusion in a medium range forecast model, *Mon. Weather Rev.*, *124*, 2322–2339, 1996.

Iqbal, M., *An Introduction to Solar Radiation*, Academic, San Diego, Calif., 1983.

Kumar, L., A. Skidmore, and E. Knowles, Modelling topographic variation in solar radiation in a GIS environment, *Int. J. Geogr. Inf. Sci.*, *11*(5), 475–497, 1997.

Mahfouf, J., E. Richard, and P. Mascart, The influence of soil and vegetation on the development of mesoscale circulations, *J. Clim. Appl. Meteorol.*, *26*, 1483–1495, 1987.

Mahrer, Y., and R. A. Pielke, A numerical study of airflow over irregular terrain, *Beitr. Phys. Atmos.*, *50*, 98–113, 1977.

Mass, C., and Y. Kuo, Regional real-time numerical weather prediction: Current status and future potential, *Bull. Am. Meteorol. Soc.*, *79*, 253–263, 1998.

Oliver, H., Studies of surface-energy balance of sloping terrain, *Int. J. Climatol.*, *12*(1), 55–68, 1992.

Oncley, S., and J. Dudhia, Evaluation of surface fluxes from MM5 using observations, *Mon. Weather Rev.*, *103*, 2281–2292, 1995.

Skartveit, A., and J. Olseth, Modelling slope irradiance at high latitudes, *Sol. Energy*, *36*(4), 333–344, 1986.

Skartveit, A., and J. Olseth, A model for the diffuse fraction of hourly global radiation, *Sol. Energy*, *38*(4), 271–274, 1987.

Stull, R., *An Introduction to Boundary Layer Meteorology*, Kluwer Acad., Norwell, Mass., 1988.

Varley, M., K. Beven, and H. Oliver, Modelling solar radiation in steeply sloping terrain, *Int. J. Climatol.*, *16*, 93–104, 1996.

Viterbo, P., A. Beljaars, J.-F. Mahfouf, and J. Teixeira, The representation of soil moisture freezing and its impact on the stable boundary layer, *Q. J. R. Meteorol. Soc.*, *125*, 2401–2426, 1999.

Warner, T., D. Kibler, and R. Steinhart, Separate and coupled testing of meteorological and hydrological forecast models for the Susquehanna River Basin in Pennsylvania, *J. Appl. Meteorol.*, *30*, 1521–1533, 1991.

Wilks, D., *Statistical Methods in the Atmospheric Sciences*, Academic, San Diego, Calif., 1995.

G. Hauge, Geophysical Institute, University of Bergen, Allegaten 70, 5007 Bergen, Norway. (gard@gfi.uib.no)

L. R. Hole, Norwegian Institute for Air Research, Instituttveien 18, P. O. Box 100, N-2027 Kjeller, Norway.